Response-based time-invariant methods for damage localization on a concrete bridge

Authors: Pier Francesco Giordano*, Maria Pina Limongelli

Department of Architecture, Built environment and Construction engineering (*DABC*), *Politecnico di Milano, Piazza Leonardo da Vinci, 32, 20133, Milan, Italy.*

*Corresponding author – Email: pierfrancesco.giordano@polimi.it

Abstract. This paper is integral part of the Special Issue on "Existing Concrete Structures: Structural Health Monitoring and Testing for condition assessment". It deals with Vibration-Based Methods (VBMs) for damage localization that approach the problem of structural integrity management through the analysis of the dynamic response of the structure under ambient or forced vibrations. In the last years, these methods received a widespread interest in the Structural Health Monitoring (SHM) community due to the possibility to use them for continuous SHM and real time damage identification. The performance of these methods is commonly verified on numerical models or laboratory specimens that, by their nature, cannot reproduce all the sources of uncertainties found in practice. The availability of data recorded on a real benchmark, the S101 bridge in Austria, enabled the comparison of three well known vibration-based time-invariant methods for damage localization, namely the curvature method, the interpolation error method, and the strain energy method. The bridge, built in the early 1960, is a typical example of a European highway bridge. Responses to ambient vibrations were recorded both in the undamaged and in several different damage scenarios artificially inflicted to the bridge. This paper reports the results of the application of the three mentioned methods of damage localization to this case study.

1 Introduction

In the last twenty years VBMs for SHM have received increasing attention by both academics and operators, due to broadly recognized advantages they provide for damage identification purposes. These are mainly related to the capability of providing continuous information about the global state of a structure without a prior knowledge about the location of possible damages and without the need to access the damaged portion of the structure. A quantification of the economic benefit provided by VBMs is not carried out in this paper, but the interested reader can refer to References [1, 2, 3]. The possibility to detect damage using responses measured by sensors not necessarily deployed close to the – unknown – location of damage is one of the major advantages of the VBMs. Damage is defined as a change introduced into a system that adversely affects its performance [4]. For VBMs damage is intended as a loss of stiffness. In fact, these methods are not indicated to identify strength reductions unless a correspondent loss of stiffness occurs. These methods rely on the fact that a reduction of stiffness results in a change of the dynamic behaviour of the structure. Therefore, structural responses to forced or ambient vibrations can be used to retrieve information about such change. Structural alterations that can be detected in principle through VBMs include all possible sources of stiffness

variations: material and/or geometric property changes, changes in boundary conditions and changes in connections between structural constituents.
It is underlined that damage can be described only by means of an indicator defined through the comparison of two structural states: a reference one (usually the state of the structure when monitoring starts) and the current state (inspection state). The damage indicator is defined in terms of the difference between the values of a parameter sensitive to damage (damage feature) in the two states.
Different levels of refinement in the identification of damage are possible, depending on the amount of information provided by the available measures. The traditional classification of methods, originally proposed by Ritter [5], distinguishes four levels of damage identification: detection, localization, quantification and prognosis. Detection, that is the identification of the presence of a damage, might be possible based on a single sensor able to capture meaningful characteristics of the structural response, e.g. the modal frequencies. Localization, that is the determination of the geometric location of damage, requires information about the structural shape. Modal or operational shapes are often used to extract damage features. In order to provide enough spatial resolution of such damage features, enabling a more accurate damage localization, a higher number of sensors deployed on the structure is usually needed. The quantification of damage, that is the estimation of its severity, usually requires a Finite Element (FE) model of the structure that allows to map the damage parameters to different damage types and scenarios, through the physical model of the geometry and mechanical characteristics of the real structure. The fourth level of Rytter's classification, i.e. prognosis, requires models of the future evolution of damage/degradation under given external actions. For the first two levels of damage identification - detection and localizations - model-based and response-based methods have been proposed in literature.
Model-based methods use FE models that are updated using experimental responses: the parameters of the model are corrected minimizing an objective function defined in terms of the discrepancy between the recorded responses and the responses simulated by the FE model. In reference [6], a comprehensive survey of model-based VBMs is reported. They have usually a considerable computational cost, due to the need to update the model parameters through iterative optimization processes. In order to overcome this problem different approaches based on substructure methods, neural networks or surrogate models have been proposed. Substructure methods allow to build a fine model for the vicinity of the damage (see for example in reference [7]) whereas neural networks identify a correspondence between the structural parameters and the structural response allowing to solve the inverse problem of updating the model parameters without utilizing the sensitivity matrix needed by FE models approach [8]. Surrogate models replace the structure model with an approximation model which usually is a polynomial function describing the relationship between the structural response and the model parameters. Some examples are the response surface method [9], the Kriging method [10], the radial basis function method [11] and feed-forward neural network [12].
Response-based methods use models based solely on the measured structural response. Damage-features are extracted from the vibrational response in terms of e.g. accelerations, and their changes are used to identify damage. The main advantage of response-based methods with respect to model-based methods is that they do not require a FE model. Therefore, the computational effort is greatly reduced. Depending on the signal-processing tool used to extract

the damage features from the response to vibrations, response-based methods can be classified in Time-invariant, in the frequency or time domain, and Time-variant methods.
In the frequency domain, Time-invariant methods use Fourier analysis as the primary signal-processing tool and time-invariant models to describe the structural behaviour. Damage features are usually defined in terms of modal parameters, mainly combinations of frequencies, modal shapes and their derivatives [13, 14, 15, 16, 17, 18, 19] or in terms of Operational Deformed Shape (ODS) retrieved from Frequency Response Functions (FRFs) [20, 21, 22, 23, 24, 25]. Time-invariant methods that operate in the time domain use statistical tools to develop mathematical models of the structural response, based on the internal structure of the recorded data. A model - with parameters calibrated on the past measured response of the structure - is used to interpret the time history of the response and the residual between the model output and the measured time history is assumed as damage feature. Auto-Regressive (AR) models or Auto-Regressive model with eXogenous inputs (ARX) models are used to model the structural response [26, 27, 28, 29]. Time-variant methods develop time-variant models that allow to identify sudden changes in the structural characteristics. They can be classified into three major groups: time-dependent models using models with time-dependent coefficients (Kalman filter), time–frequency methods that analyze time variations of the spectral quantities using, for example, the Wigher-Ville distribution and time–scale methods that decompose the signal based on a priori chosen functions, e.g. wavelets. A review of these methods can be found in reference [30].
Two main differences emerge when comparing response based and model-based methods, namely: a) model-based methods are more demanding due to the need of building and updating a FE model. This makes them less suitable for real-time structure damage identification with respect to response-based method; b) a more detailed description of damage - including also quantification and prognosis - is enabled by model-based methods whereas response-based methods are usually limited to the first two levels of damage identification, i.e. detection and localization.
To the aim of continuously monitor the structural health and have early warnings about possible damages, response-based damage detection methods are more efficient and, for large structures, the possibility to locate the damaged portion of the structure enables targeted interventions. The idea underlying most of the methods for the localization of stiffness losses is that, since a localized reduction of stiffness alters the structural deformed shape, damage can be identified by processing the geometric changes of this shape. The irregularity induced by a stiffness loss affects the global deformed shape. In the following, three response-based time invariant methods for damage localization, based on either modal shapes or ODSs, are described. Each method uses a different damage feature, but they are all related to the shape curvature and they all define the damage indicator in terms (difference or ratio) of the change of the damage feature.
One of the main issues in the research field related to damage localization is the validation on real structures of the methods proposed by researchers. The number of monitored structures is still low and usually, due to economic constraints, a small amount of sensors is deployed on them. Beside this, many of the instrumented structures have never experienced damage and, in some cases, even if records exist, they are not freely available for research purposes. Due to all these facts, the methods proposed in literature for damage localization are often verified using

data simulated using numerical models or obtained through tests of scaled laboratory specimens. Furthermore, each method is usually applied to a different case study and the direct comparison of several methods using the same case study has been performed in a very limited number of cases. Notable examples are the I-40 bridge over the Rio Grande in Albuquerque, NM, [31] and the Z24 bridge, over the A1 highway between Bern and Zürich in Switzerland [32].

In this paper, the performance of three well known response-based time-invariant methods for damage localization is compared using structural responses measured in terms of accelerations. Responses recorded on the Flyover Reibersdorf S101 bridge, in Austria, were used to this aim. The considered methods include the curvature method [33], the strain energy method [34] and the interpolation error method [35] that are applied formulating the damage indicator both in terms of modal shapes and in terms of ODSs. The goal is to demonstrate which method is more suitable for preliminary damage localization based on responses measured in terms of acceleration. Recent studies [36] demonstrated that the use of strains enables a more reliable estimate of the damage indicators. However, the structural response is measured more frequently in terms of accelerations rather than strains. Therefore, herein the focus is on the application of damage localization methods base on acceleration records.

After this introductory section, the paper is organized as follows. The second section is dedicated to the presentation of the three damage localization methods, which are formulated in terms of both modal shapes and ODSs. The third section is focused on the presentation of the case study and includes the descriptions of the bridge and the tests carried out on the structure before its demolition. The fourth section presents the analysis of the response of the bridge under ambient vibration during the test, including estimation of frequencies, modal shapes and ODSs. The fifth section offers the comparison of results obtained using different methods on the basis of the accuracy of the damage localization. Additional comparison of results relates to the damage features computed in terms of modal shapes and ODSs (comprehensive results are shown in the Annex). The sixth and last section is devoted to conclusions.

2 Damage localization methods

The principal aim of most methods for damage localization based on modal shapes is to find an irregularity (presumably induced by damage) in the deformed shapes that was not present in the reference configuration. Similar considerations can be made considering the ODSs obtained from FRFs, which provide spatial information on the vibration shape of the structure in the frequency domain. Both modal shapes and ODSs can be estimated by processing acceleration records measured at locations where sensors are deployed, thus in a limited number of locations. Under ambient vibration, i.e. in absence of artificial excitation, the estimation of modal shapes can be carried out by Time-domain or Frequency-domain OMA techniques [37]. ODSs can be obtained from FRFs of the measured responses with respect to the known input excitation or, in case of ambient excitation, from the Power Spectral Densities (PSDs) of the responses. The three damage localization methods considered in this work are formulated in the following subsections in term of both modal shapes and ODSs. The curvature and the strain energy

methods were originally formulated in terms of modal shapes whereas the interpolation error method was formulated in the terms of ODSs. The curvature method and the strain energy method require the explicit computation of the modal curvature that can be numerically estimated from the deformed shapes at the locations were sensors are located through numerical methods such as the central difference approximation of the second derivative. In the case of unevenly spaced sensors, as for the vibration tests on the S101 bridge described in Section 3, the curvature $\phi''_{k,i}$ of the *k*-th modal shape at the *i*-th location can be computed, as follows

$$\phi''_{k,i} = \frac{\left(\frac{\phi_{k,i+1} - \phi_{k,i}}{x_{i+1} - x_i}\right) - \left(\frac{\phi_{k,i} - \phi_{k,i-1}}{x_i - x_{i-1}}\right)}{\left(\frac{x_{i+1} - x_{i-1}}{2}\right)} \tag{1}$$

where $\phi_{k,i}$ is the component of the *k*-th modal shape at the *i*-th location and x_i is the longitudinal coordinate of the same component along the bridge deck. The curvature $H''_{k,i}$ of the k-th ODS, $H_{k,i}$, at the *i*-th location can be estimated in similar manner as

$$H''_{k,i} = \frac{\left(\frac{H_{k,i+1} - H_{k,i}}{x_{i+1} - x_i}\right) - \left(\frac{H_{k,i} - H_{k,i-1}}{x_i - x_{i-1}}\right)}{\left(\frac{x_{i+1} - x_{i-1}}{2}\right)} \tag{2}$$

The modal curvature might be evaluated directly, i.e. avoiding the numerical differentiation, and therefore more accurately when measurements from optical fiber strain sensors are available [36]. The interpolation method does not require an explicit computation of the modal curvature.

2.1 Variation of curvature

Pandey et al. [13] showed that the absolute changes in the curvature of modal shapes between a reference and a damage configuration is an indicator of stiffness losses due to the direct relationship between curvature and bending stiffness. Therefore, changes in the curvature can be used to detect and locate damage. The sum, over all the identified modes $k = 1,...,n_{modes}$, of the absolute variations of modal curvature, Δc_i, between a reference, $\phi''_{k,i,U}$, and the current (i.e. possibly damaged) state, $\phi''_{k,i,D}$, at the *i*-th instrumented location (that is one of the $i = 1,...,N$ locations where the components of the modal shapes are estimated) is assumed as damage-sensitive feature at location i, as follows:

$$\Delta c_i = \sum_{k=1}^{n_{modes}} \left| \phi''_{k,i,D} - \phi''_{k,i,U} \right| \tag{3}$$

The expression of the damage-sensitive feature at the *i*-th location formulated in terms of ODSs reads

$$\Delta c_i = \sum_{k=1}^{n_{freq}} \left| H''_{k,i,D} - H''_{k,i,U} \right| \tag{4}$$

where $k = 1,...,n_{freq}$ is the number of ODSs; $H''_{k,i,U}$ is the curvature of the k-th ODS in the reference configuration at the *i*-th location; and $H''_{k,i,D}$ is the curvature of the k-th ODS in the current configuration at the *i*-th location.

2.2 Variation of modal interpolation error

The interpolation error can be used to measure the smoothness of the modal shapes: a small interpolation error corresponds to high smoothness. A local change of curvature (due to a loss of stiffness) creates a reduction of smoothness and therefore an increase of the interpolation error. The variation of this parameter has been proposed as damage feature by Limongelli [24]. The interpolation error is defined analytically as the error related to the interpolation of the *k*-th modal shape with a smooth function, specifically a cubic spline. Due to the so-called "Gibbs phenomenon for splines", a sharp increase of the interpolation error can be observed at the locations with a curvature discontinuity and this can be used to detect the locations where a loss of stiffness have occurred. At the *i*-th instrumented location, the accuracy of the interpolation is computed for the *k*-th mode through the interpolation error, $E_{k,i} = \left| \phi_{k,i} - \hat{\phi}_{k,i} \right|$, that is the absolute variation between the measured component of the *k*-th modal shape at that location, $\phi_{k,i}$, and the interpolated value of the same component, $\hat{\phi}_{k,i}$. The contributions of all the identified modes are combined at the *i*-th location, as follows:

$$E_i = \sqrt{\sum_{k=1}^{n_{modes}} E_{k,i}^2} = \sqrt{\sum_{k=1}^{n_{modes}} \left| \phi_{k,i} - \hat{\phi}_{k,i} \right|^2} \tag{5}$$

The increase of the interpolation error at a given location with respect to the reference state highlights a decrease in the accuracy of the interpolation, which indicates a change of stiffness at that location. The damage-sensitive feature ΔE_i is formulated as

$$\Delta E_i = E_{i,D} - E_{i,U} = \sqrt{\sum_{k=1}^{n_{modes}} \left| \phi_{k,i,D} - \hat{\phi}_{k,i,D} \right|^2} - \sqrt{\sum_{k=1}^{n_{modes}} \left| \phi_{k,i,U} - \hat{\phi}_{k,i,U} \right|^2} \tag{6}$$

where $E_{i,U}$ and $E_{i,D}$ represent the modal interpolation error at the *i*-th location (obtained by means of Eq. 5) computed in a reference and the possibly damage state, respectively. The damage-sensitive feature expressed in terms of ODSs reads

$$\Delta E_i = E_{i,D} - E_{i,U} = \sqrt{\sum_{k=1}^{n_{freq}} \left| H_{k,i,D} - \hat{H}_{k,i,D} \right|^2} - \sqrt{\sum_{k=1}^{n_{freq}} \left| H_{k,i,U} - \hat{H}_{k,i,U} \right|^2} \tag{7}$$

where $\hat{H}_{k,i,U}$ and $\hat{H}_{k,i,D}$ are the interpolated values of the *k*-th ODS at the *i*-th location in a reference and the possibly damage state, respectively.

2.3 Modal strain energy ratio

The fraction of modal strain energy is defined as the ratio between the modal strain energy stored in the *i*-th element and the modal strain energy stored in the structure. The damage localization feature proposed by Stubbs [34] is based on the assumption that the damage does not change the fraction of modal strain energy stored in each sub-element of the structure between the undamaged and the damaged states. Under this hypothesis, the ratio between the bending stiffness of the *i*-th element in the undamaged *U* and in the damaged *D* states can be computed as a function of the modal curvatures. Summing up the contributions of all the identified modes, the damage-sensitive feature β_i is obtained at the *i*-th location, as follows:

$$\beta_i = \sum_{k=1}^{n_{modes}} \frac{\phi''_{k,i,D}{}^2}{\sum_{i=1}^{N} \phi''_{k,i,D}{}^2} \Big/ \sum_{k=1}^{n_{modes}} \frac{\phi''_{k,i,U}{}^2}{\sum_{i=1}^{N} \phi''_{k,i,U}{}^2} \tag{8}$$

The damage-sensitive feature assumes values higher than 1 at locations where a reduction of the bending stiffness has occurred in the damaged state. In similar fashion, the damage feature defined in terms of ODSs is given by the following expression:

$$\beta_i = \sum_{k=1}^{n_{freq}} \frac{H''_{k,i,D}{}^2}{\sum_{i=1}^{N} H''_{k,i,D}{}^2} \Big/ \sum_{k=1}^{n_{freq}} \frac{H''_{k,i,U}{}^2}{\sum_{i=1}^{N} H''_{k,i,U}{}^2} \tag{9}$$

3 Case study: the S101 bridge

The case study considered in this paper to compare the three damage localization algorithms is the S101 bridge, a prestressed concrete bridge built in the early 1960 in Reibersdorf, west of Vienna, Austria. The total length of the bridge was 56 m with a main span 32 m long and two side spans 12 m long. The deck was 7.2 m wide, made of a double-webbed t-beam of variable height, from 0.9 m at mid span to 1.7 m in proximity of the piers. A lateral view of the bridge is shown in Figure 1.

Figure 1: Lateral view of the bridge

The bridge was demolished in 2008, almost 50 years after its construction, due to insufficient loading capacity and bad maintenance conditions and also to allow the enlargement of underneath A1 Westautobahn. Before the demolition, an experimental campaign was carried out in the realm of the IRIS project [38]: the structure was progressively damaged, and the dynamic response to ambient vibrations was registered for 3 consecutive days between the 10th and the 13th December 2008. Two major types of damages were inflicted on the bridge. First, the north-western pier (highlighted in Figure 1) was cut and progressively lowered to simulate a settlement. Then, an increasing number of tendons was cut to simulate prestress loss. Several research groups used the data recorded on this bridge for research purposes [39, 40, 41].
In this paper, only data relevant to the settlement of the pier are considered. In fact, the cut of the tendons caused only minor variations of the section stiffness that cannot be identified by vibration-based damage identification algorithms, as demonstrated in reference [41]. The description of the stepwise damage evolution is reported in Table 1. First, the pier was cut above the foundation (Scenario A). A hydraulic jack was placed underneath the pier while the structure was secured by a supporting pier. After that, the pier was progressively settled, until a final lowering of about 3 cm (Scenario D). The last step of the test (Scenario E) concerns the simulation of a repair: the bridge was lifted using the hydraulic jack and compensating plates were inserted to keep the pier in the final position. More detailed information about the bridge and the experimental tests can be found in reference [42]. The choice of this case study is driven by the availability of responses to ambient vibrations recorded during the three days of test that enabled the application of the three considered methods of damage localization in terms of both modal and ODSs as it is described in the following sections.

Table 1. Progressive damage test

Scenario	Start	End	Description of inflicted damage
U	10.12.2008 (05:16 PM)	11.12.2008 (07:13 AM)	Undamaged structure
A	11.12.2008 (07:13 AM)	11.12.2008 (10:21 AM)	Cut of the north-western column
B	11.12.2008 (10:21 AM)	11.12.2008 (11:49 AM)	First lowering the column (1cm)
C	11.12.2008 (11:49 AM)	11.12.2008 (01:39 PM)	Second lowering the column (2cm)
D	11.12.2008 (01:39 PM)	11.12.2008 (02:45 PM)	Third lowering the column (3cm)
E	11.12.2008 (02:45 PM)	12.12.2008 (05:52 AM)	Insertion of compensating plates

4 Analysis of the response to ambient vibrations

The response of the S101 bridge to ambient vibrations was recorded in terms of acceleration by the 15 triaxial sensors deployed as shown in Figure 2. Fourteen accelerometers were placed on the west side of the deck plus one accelerometer on the opposite side to detect torsional modes. In this work, only vertical accelerations recorded by the sensors placed on the west side are used to compute the different damage-sensitive features (500 Hz sampling rate – 60 min recording length for the undamaged scenario and each damage scenario). Data from sensor 4 are not available, therefore the modal shapes cannot be estimated at that location. The analysis of natural frequencies, modal shapes and ODSs is discussed in the following subsections.

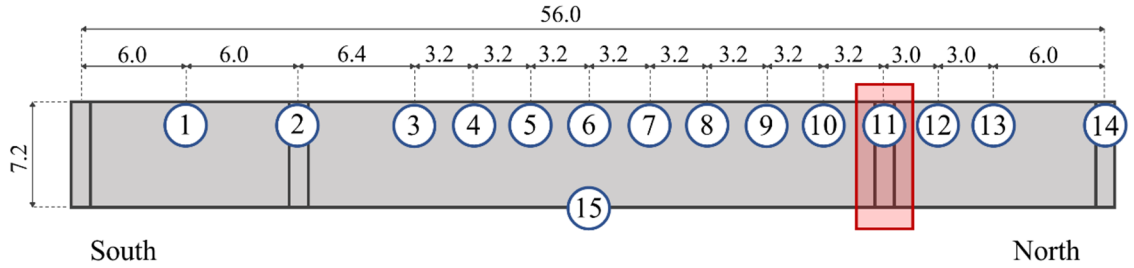

Figure 2: Location of sensors on the deck of the S101 bridge, quotes in [m]. The location of damage, in proximity of sensor 11, is highlighted in red

4.1 Natural frequencies and modal shapes

Natural frequencies and modal shapes are identified by using the EFDD technique available in the software ARTeMIS. Only the first three identified vibration modes are considered in the calculation of the damage-sensitive features since the higher modes cannot be identified accurately. The values of the identified modal frequencies are reported in *Table 2* for the reference (undamaged) and all the damaged scenarios, together with the values of their percentage variation with respect to the value in the undamaged state. As expected, the modal frequencies decrease with the augmentation of damage from Scenarios U to D. Modal frequencies increase in Scenario E, corresponding to the simulated repair of the pier. However, they do not recover the original values indicating that permanent damage was induced in the bridge by the previous settlements. The real components of the modal shapes of the first three modes are displayed in Figure 3. The first and third mode are bending modes whereas the second one is a torsional mode. The evolution of these shapes with damage shows clearly the change of configuration that occurs in proximity of the damaged location due to the pier settlement: the modal shapes progressively deviate from the undamaged profile (dark blue line) with increasing damage severity. Similar results were found in previous studies [42].

Table 2. Modal frequencies in the undamaged and in the damaged scenarios

Scenario	f_1 [Hz]	Δf_1 [%]	f_2 [Hz]	Δf_2 [%]	f_3 [Hz]	Δf_3 [%]
U	4.04	-	6.28	-	9.67	-
A	4.03	-0.25	6.27	-0.16	9.67	0.00
B	3.90	-3.47	6.03	-3.98	9.39	-2.90
C	3.92	-2.97	5.79	-7.80	9.27	-4.14
D	3.75	-7.18	5.34	-14.97	8.57	-10.64
E	3.94	-2.48	5.79	-7.80	9.09	-6.00

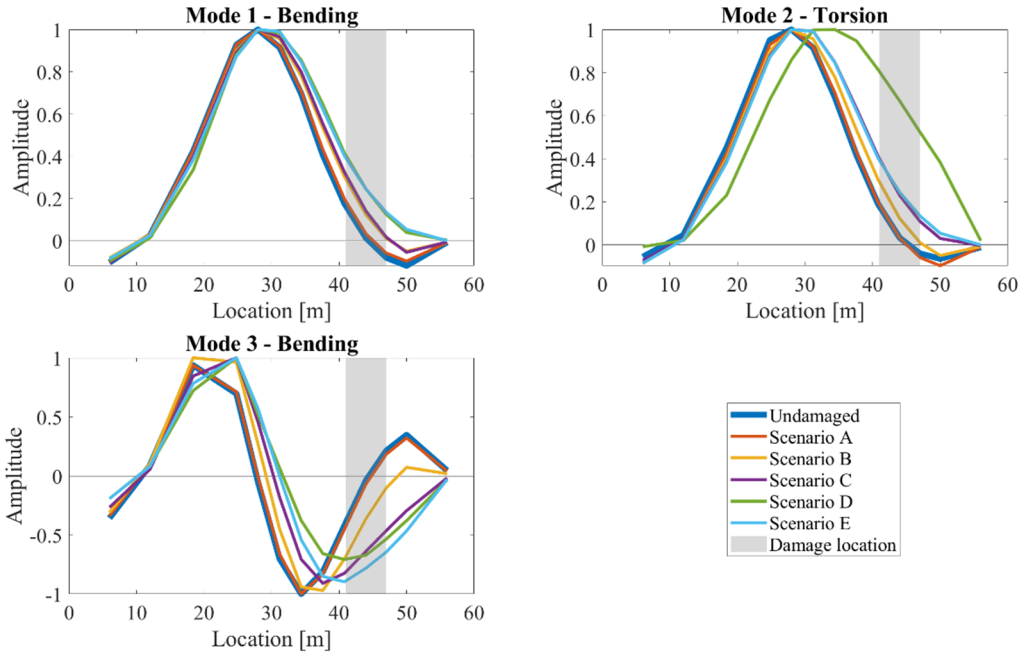

Figure 3: Modal shapes of the first three modes

4.2 Operational Deformed Shapes

The ODSs are obtained by considering the PSD of the acceleration records at the location of sensors, for each scenario. In order to reduce the effect of noise, the Welch method is applied to compute the PSDs. This method is based on the averaging the square magnitude of the Discrete Fourier Transform (DFT) of portions of the acceleration records: the recorded sample is divided in n_d overlapping blocks of size S, shifted each other of S_{shift}. The length S of the blocks (taken as a power of 2 to improve the performances of the procedure) determines the frequency resolution Δf ($\Delta f = 1/(S\Delta t)$, where Δt is the inverse of the sampling frequency) of the PSD, whereas the number of blocks depends on the overlap between blocks. To reduce the effect of leakage, a Hamming window of size S is applied to each block. The parameters chosen for the analysis are $S = 8192$ and 50% overlapping. The PSDs estimated at location 11, i.e. in correspondence to the settled pier, for all the considered scenarios are shown in Figure 4. The focus in Figure 4 is in the frequency range 0-10 Hz, where the first three identified modal frequencies lie.

In the undamaged Scenario U, the PSDs (therefore the amplitudes of the modal component) are null since this location – where the pier is located - corresponds to a node for all the three modes. When the damage is inflicted to the column, the PSD exhibits peaks near 4, 6 and 9 Hz, according to the corresponding modal frequencies shown in Table 2.This effect is due to the change in the deformed profile due to the occurrence of damage that deviates the position of the node from location 11.

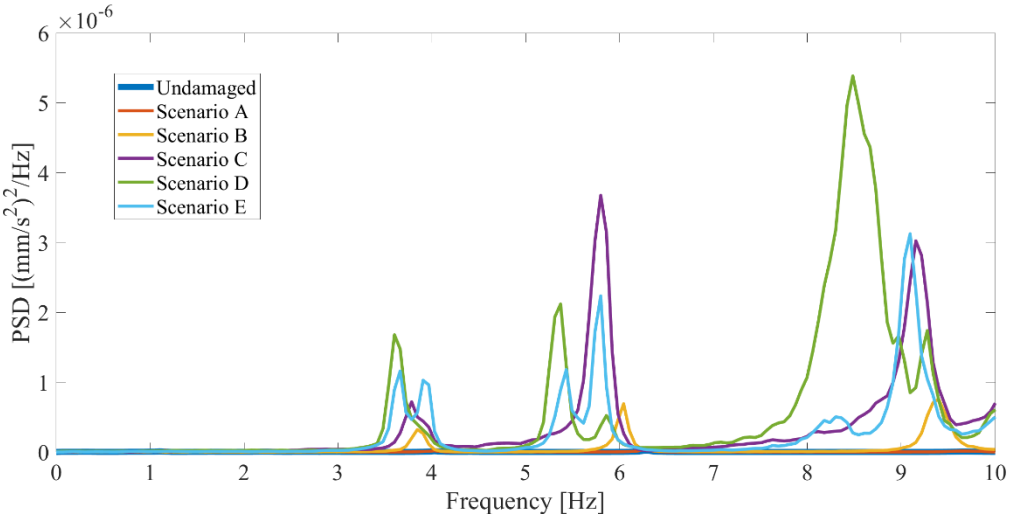

Figure 4: PSD estimated at location 11 for all the scenarios

5 Comparison of damage localization features

The three damage localization methods presented in Section 2 are applied to the five damage scenarios described in Table 1. The curvature of modal shapes and ODSs is computed by means of the central difference approximation method introduced in Section 2. Instead, the damage feature based on the interpolation error can be calculated directly. Note that by using the central difference approximation method for the computation of the curvature, the damage-sensitive feature cannot be computed in correspondence of sensor 1 and 14. Also the interpolation error method, as it is formulated, does not allow to compute the damage-sensitive feature at the sensors located at the ends. Figure 5 shows the three damage features computed in terms of modals shapes. Figure 6 displays the damage-sensitive features based on the ODSs computed in the range 0-30 Hz. The different damage-sensitive features have been normalized so that the maximum value is equal to 1 in order to ease the comparison of results.
In these figures, the grey bars indicate the position of the settled pier, that is the portion of the structure where damage is located. The dashed horizontal lines indicate the values of the thresholds, computed as a percentile of the distribution of the values of each damage feature in the damaged configuration. Theses thresholds are used to classify a location as damaged or undamaged. Specifically, assuming a Gaussian distribution of the damage indicator over the instrumented locations, each threshold is computed as

$$I_T = \mu_I + \nu\sigma_I \tag{10}$$

where μ_I and σ_I are the mean and the standard deviation, respectively, of the sample population of the damage feature; the parameter ν defines the percentile chosen to classify damaged locations. The classification of a certain location i as a "damaged" is carried out by comparing the current value of the damage feature I_i and the corresponding threshold I_T

$$\text{if } I_i - I_T > 0 \qquad \text{damage at location } i \tag{11}$$

if $I_i - I_T \leq 0$ no damage at location i

Herein, the threshold is computed assuming $\nu = 1$, corresponding to 65% percentile. The quantitative comparison of the results provided by the three damage-sensitive features is performed by means of the relative error e_L [43], which expresses the relative distance between the real and the identified damage location, normalized by the length L of the bridge as follows:

$$e_L = \frac{x_R - x_I}{L} \times 100 \tag{12}$$

where x_R and x_I are the coordinates along the bridge axis of the real and the identified damage location, respectively . The real damage position is located at $x_R = 44\,\text{m}$, in correspondence of sensor 11. The identified damage location in Equation (12) corresponds to the maximum value of the indicator exceeding the threshold. The values of the relative error e_L are shown in Table 3 and Table 4 for the features computed in terms of modal shapes and ODSs, respectively. Negative values of the relative error indicate that the maximum value of the damage feature is located on the right with respect to the actual damage position ($x_R < x_I$). Positive values mean that it is located on the left ($x_R > x_I$). Note that the damage locations are identified at discrete points along the bridge deck, where sensors are located. For instance, the value $e_L = 5.71$ means that the maximum value of the damage feature is located at sensors 10 (one sensor distance). The values in brackets reported in *Table 3* and *Table 4* indicates the distance in terms of sensors between sensors 11 and the sensors where the peak of the damage feature is located.

The interpolation error method and the strain energy method provide similar results when formulated in terms of modal shapes. The curvature method is not able to correctly localize damage in any scenario. In Scenario D, the interpolation error method gives false alarms in locations far from damage, where few accelerometers are installed. The results of the interpolation error method improve when using ODSs. In the Annex, the damage-sensitive features computed considering different frequency ranges for the computation of ODSs are displayed, see Figures 7-11. The results provided by the interpolation error method are stable with increasing frequency range. Occasionally, damage is not localized in Scenario A, which is the less severe. On the other hand, the results given by the strain energy method are very sensitive to the considered frequency range. Overall, the strain energy method does not localize damage on the structure reliably when formulated using ODSs.

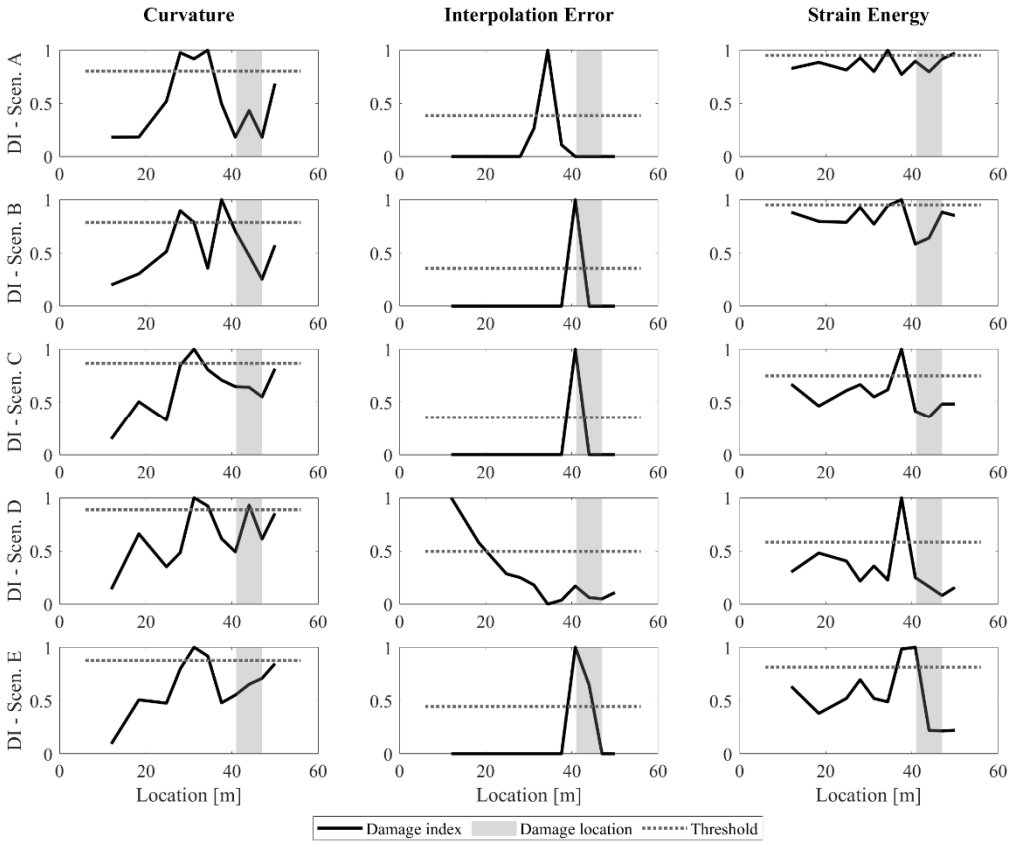

Figure 5: Damage features for different damage scenarios formulated in terms of modal shapes

Table 3. Relative error e_L [in %] using modal shapes

Method	Scenario				
	A	B	C	D	E
Curvature	17.14 (3)	11.43 (2)	22.86 (4)	22.86 (4)	22.86 (4)
Interpolation error	17.14 (3)	5.71 (1)	5.71 (1)	57.14 (9)	5.71 (1)
Strain energy	17.14 (3)	11.43 (2)	11.43 (2)	11.43 (2)	5.71 (1)

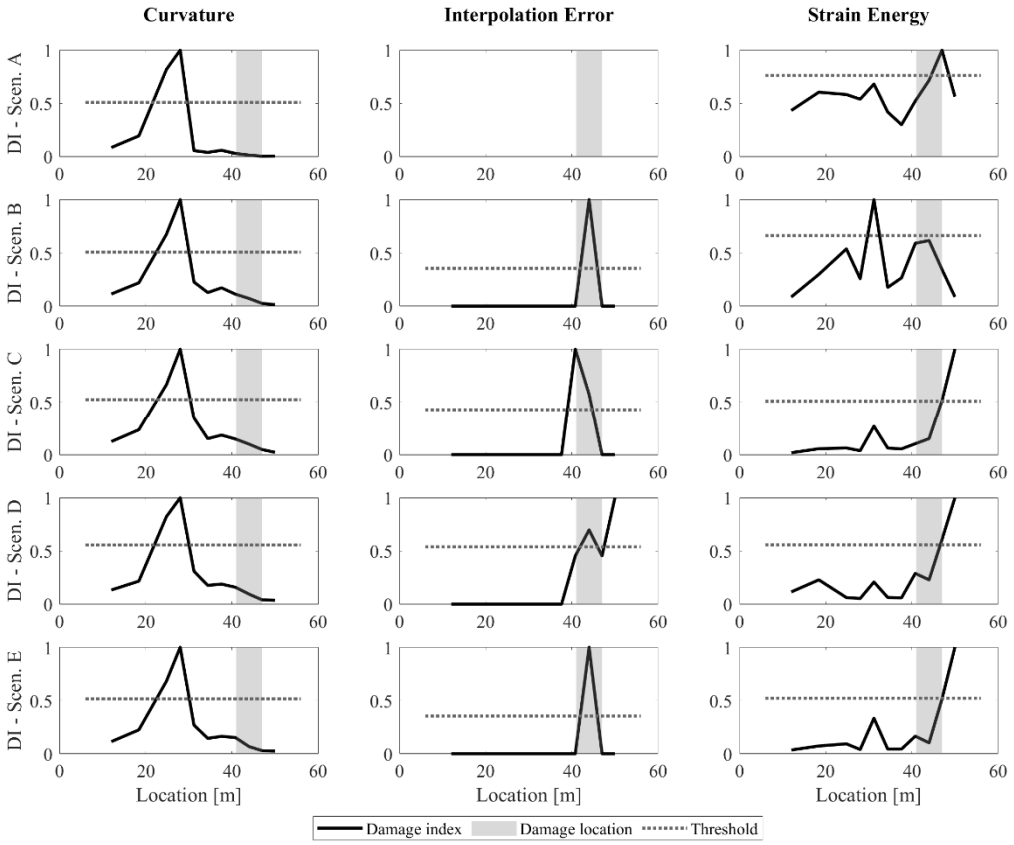

Figure 6: Damage features for different damage scenarios formulated in terms of ODSs (frequency range 0-30Hz)

Table 4. Relative error e_L [in %] using ODSs (frequency range 0-30 Hz)

Method	Scenario				
	A	B	C	D	E
Curvature	28.57 (5)	28.57 (5)	28.57 (5)	28.57 (5)	28.57 (5)
Interpolation error	5.71 (1)	5.71 (1)	5.71 (1)	5.71 (1)	5.71 (1)
Strain energy	22.86 (4)	5.71 (1)	22.86 (4)	45.71 (8)	5.71 (1)

6 Conclusions

In this paper, the results of the application of three response-based methods for damage localization to the benchmark S101 bridge in Austria are reported. The three methods, applied using responses recorded in terms of acceleration, are the curvature method, the interpolation error method and the strain energy method. The damage features have been computed in terms of both modal shapes and ODSs and compared for five damage scenarios of varying severity. The comparison is performed in terms of the localization error defined in terms of the relative distance between the real and the identified damage location. The strain energy method and the

interpolation method provide comparable results using modal shapes whereas, in general, the curvature method is not able to correctly locate damage. The damage-sensitive features are formulated in terms of ODSs, for multiple frequency ranges. The performance of the interpolation error method increases when the method is formulated in terms of ODSs. The results of the curvature method and the strain energy methods vary according to the considered frequency range. In general, these two methods are not able to locate damage when formulated using ODSs. The damage-sensitive feature based on the interpolation error is preferable for the purpose of preliminary and real time damage identification since it can be retrieved directly from the PSDs of the recorded responses without the need of modal identification. Further investigations, such as visual inspections or model-based techniques should be used at a later time for a more precise damage localization and assessment.

Acknowledgements

The authors would like to thank the Vienna Consulting Engineers (VCE) company for providing the experimental data recorded during the tests on the S101 bridge.
This study was partially funded by the Italian Civil Protection Department within the project DPC-RELUIS 2019 - RS4 ‘Monitoring and satellite data’.

References

[1] P. Giordano, L. Prendergast and M. Limongelli, "A framework for assessing the value of information for health monitoring of scoured bridges," *Journal of Civil Structural Health Monitoring,* 2020.

[2] L. Iannacone, P. Gardoni, P. Giordano and M. Limongelli, "Decision Making Based on the Value of Information of Different Inspection Methods," in *Proceedings of the 12th International Workshop on Structural Health Monitoring (IWSHM 2019)*, Stanford, Stanford University, 2019.

[3] D. Zonta, B. Glisic and S. Adriaenssens, "Value of information: impact of monitoring on decision-making," *Structural Control and Health Monitoring,* vol. 21, p. 1043–1056, 2014.

[4] C. Farrar and K. Worden, "Structural Health Monitoring: a machine learning perspective," John Wiley & Sons, Ltd, Chichester, West Sussex, United Kingdom, 2013.

[5] A. Rytter, "Vibrational Based Inspection of Civil Engineering Structures," University of Aalborg, PhD thesis, Aalborg, Denmark, 1993.

[6] J. E. Mottershead and M. I. Friswell, "Model updating in structural dynamics: A survey," *Journal of sound and vibration,* vol. 167, no. 2, p. 347–375, 1993.

[7] X. Kong, D. J. Wu, C. S. Cai and Y. Q. Liu, "New strategy of substructure method to model long-span hybrid cable-stayed bridges under vehicle-induced vibration," *Engineering Structures,* vol. 34, p. 421–435, 2012.

[8] O. Abdeljaber, O. Avci, S. Kiranyaz, M. Gabbouj and D. J. Inman, "Real-time vibration-based structural damage detection using one-dimensional convolutional neural networks," *Journal of Sound and Vibration,* vol. 388, pp. 154-170, 2017.

[9] S. Fang and R. Perera, "A response surface methodology based damage identification technique," *Smart Materials and Structures,* vol. 18, no. 6, 2009.

[10] H. Y. Gao, X. L. Guo and X. F. Hu, "Crack identification based on Kriging surrogate model," *Structural Engineering and Mechanics,* vol. 41, no. 1, pp. 25-41, 2012.

[11] V. Krishna, "Structural Optimization Using ANSYS Classic and Radial Basis Function Based Response Surface Model," Master's Thesis, Mechanical Engineering, University of Texas at Arlington, Arlington, TX, USA, 2009.

[12] P. Torkzadeh, H. Fathnejat and R. Ghiasi, "Damage detection of plate-like structures using intelligent surrogate model," *Smart Structures and Systems,* vol. 18, no. 6, p. 1233–1250, 2016.

[13] A. K. Pandey, M. Biswas and M. M. Samman, "Damage detection from changes in curvature mode shapes," *Journal of Sound and Vibration,* vol. 145, no. 2, pp. 321-332, 1991.

[14] N. Stubbs, J. Kim and K. Topole, "An efficient and robust algorithm for damage localization in offshore structures," in *10th ASCE Structures Conference, American Society of Civil Engineers*, San Antonio, Texas, 1992.

[15] C. P. Ratcliffe, "Damage Detection Using A Modified Laplacian Operator On Mode Shape Data," *Journal of Sound and Vibration,* vol. 204, no. 3, pp. 505-517, 1997.

[16] Z. Zhang and A. E. Aktan, "Application of Modal Flexibility and its Derivatives in Structural Identification," *Journal of Research in Nondestructive Evaluation,* vol. 10, no. 1, pp. 43-61, 1998.

[17] M. A. Wahab and G. De Roeck, "Damage detection in bridges using modal curvatures: application to a real damage scenario," *Journal of sound and vibration,* vol. 226, no. 2, pp. 217-235, 1999.

[18] Y. K. Ho and D. J. Ewins, "On the structural damage identification with mode shapes," *International Conference on System Identification and Structural Health Monitoring,* pp. 677-686, 2000.

[19] Q. Lu, G. Ren and Y. Zhao, "Multiple damage location with flexibility curvature and relative frequency change for beam structures," *Journal of sound and vibration,* vol. 253, no. 5, pp. 1101-1114, 2002.

[20] P. F. Pai and S. Jin, "Locating structural damage by detecting boundary effects," *Journal of Sound and Vibration,* vol. 231, no. 4, p. 1079–1110, 2000.

[21] E. Parloo, P. Guillaume and M. Van Overmeire, "Damage assessment using mode shape sensitivities," *Mechanical Systems and Signal Processing,* vol. 17, no. 3, pp. 499-518, 2003.

[22] A. Gentile and A. Messina, "On the continuous wavelet transforms applied to discrete vibrational data for detecting open cracks in damaged beams," *International Journal of Solid and Structures,* vol. 40, no. 2, pp. 295-315, 2003.

[23] A. Dutta and S. Talukdar, "Damage detection in bridges using accurate modal parameters," *Finite Elements in Analysis and Design,* vol. 40, no. 3, pp. 287-304, 2004.

[24] M. P. Limongelli, "Frequency Response Function Interpolation for Damage Detection under Changing Environment," *Mechanical Systems and Signal Processing,* vol. 24, no. 8, pp. 2898-2913, 2010.

[25] Y. Zhang, S. T. Lie and Z. Xiang, "Damage detection method based on operating deflection shape curvature extracted from dynamic response of a passing vehicle," *Mechanical Systems and Signal Processing,* vol. 35, p. 238–254, 2013.

[26] P. Fanning and E. P. Carden, "Auto-regressive and statistical process control techniques applied to damage indication in telecommunication masts," *Key Engineering Materials,* Vols. 204-205, pp. 251-260, 2001.

[27] H. Sohn and C. R. Farrar, "Damage diagnosis using time series analysis of vibration signals," *Smart Materials and Structures,* vol. 10, no. 3, p. 446–451, 2001.

[28] S. G. Mattson and S. M. Pandit, "Statistical moments of autoregressive model residuals for damage localisation," *Mechanical Systems and Signal Processing,* vol. 20, no. 3, p. 627–645, 2006.

[29] K. K. Nair, A. S. Kiremidjian and K. H. Law, "Time series-based damage detection and localization algorithm with application to the ASCE benchmark structure," *Journal of Sound and Vibration,* vol. 291, no. 1–2, p. 349–368, 2006.

[30] W. J. Staszewski and A. N. Robertson, "Time–frequency and time–scale analyses for structural health monitoring," *Philosophical Transactions of the Royal Society A,* vol. 365, p. 449–477, 2007.

[31] C. R. Farrar and D. A. Jauregui, "Comparative study of damage identification algorithms applied to a bridge: I. Experiment," *Smart materials and Structures,* vol. 7, pp. 704-719, 1998.

[32] J. Maeck, B. Peeters and G. De Roeck, "Damage identification on the Z24 bridge using vibration monitoring," *Smart Materials and Structures,* vol. 10, no. 3, pp. 512-517, 2001.

[33] A. Pandey, M. Biswas and M. Samman, "Damage detection from changes in curvature mode shapes," *Journal of Sound and Vibration,* vol. 145, no. 2, pp. 321-332, 1991.

[34] N. Stubbs, J. Kim and K. Topole, "An efficient and robust algorithm for damage localization in offshore structures," in *10th ASCE Structures Conference, American Society of Civil Engineers*, San Antonio, Texas, 1992.

[35] M. P. Limongelli, "The interpolation damage detection method for frames under seismic excitation," *Journal of Sound and Vibration,* vol. 330, no. 22, p. 5474–5489, 2011.

[36] E. Reynders, G. De Roeck, P. G. Bakir and C. Sauvage, "Damage Identification on the Tilff Bridge by Vibration Monitoring Using Optical Fiber Strain Sensors," *e Journal of Engineering Mechanics,* vol. 133, no. 2, pp. 185-193, 2007.

[37] C. Rainieri and G. Fabbrocino, Operational Modal Analysis of Civil Engineering Structures. An Introduction and Guide for Applications, New York: Springer-Verlag, 2014.

[38] H. Wenzel, IRIS - Industrial Safety and Life Cycle Engineering: Technologies, Standards, Applications, Austria: VCE Vienna Consulting Engineers, 2013.

[39] F. Hille, M. Döhler, L. Mevel and W. Rücker, "Subspace-based Damage Detection Methods on a Prestressed Concrete Bridge," in *Proceedings of the 8th International Conference on Structural Dynamics, EURODYN 2011*, Leuven, Belgium, 2011.

[40] D. Siringoringo, T. Nagayama, Y. Fujino and T. Nagayama, "Dynamic Characteristics of an Overpass Bridge in a Full-Scale Destructive Test," *Journal of Engineering Mechanics,* vol. 139, no. 6, pp. 691-701, 2013.

[41] M. P. Limongelli, M. Tirone and C. Surace, "Non destructive monitoring of a prestressed bridge with a data-driven," in *Proc. of SPIE*, 2017.

[42] VCE, "Progressive damage test S101. Flyover Reibersdorf," Report nr. 08/2308, Austria, 2009.

[43] S. Dincal and N. Stubbs, "Nondestructive damage detection in Euler-Bernoulli beams using nodal curvatures - Part I: Theory and numerical verification," *Structural Control and Health Monitoring,* vol. 21, pp. 303-316, 2014.

Annex

In this section, the damage-sensitive features computed considering different frequency ranges for the computation of ODSs are displayed, from Figure A1 to Figure A5. The plots relate to five different damage scenarios, from A to E. The investigated frequency ranges are 0-10 Hz, 0-20 Hz, 0-40 Hz, 0-50 Hz, and 0-100 Hz. The results are compared in terms of relative errors e_L, which are displayed in Table A1 through Table A5.

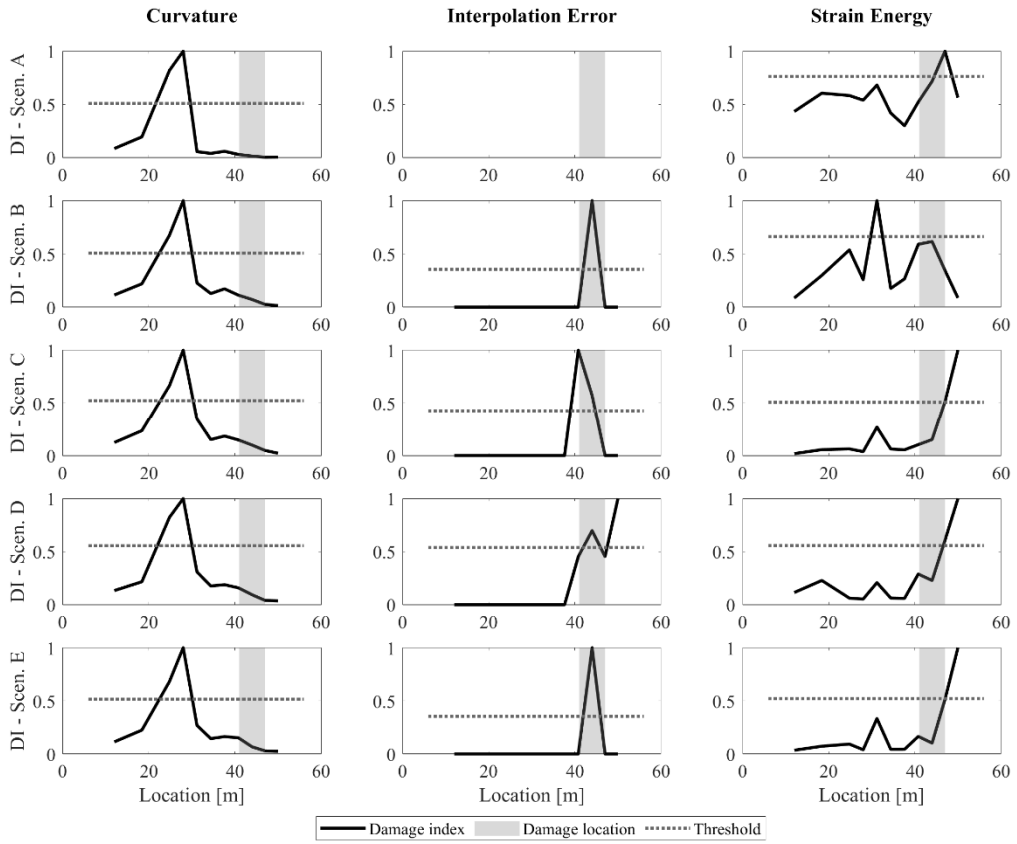

Figure A1: Damage features for different damage scenarios formulated in terms of ODSs (frequency range 0-10Hz)

Table A1. Relative error e_L [in %] using ODSs (frequency range 0-10 Hz)

Method	Scenario				
	A	B	C	D	E
Curvature	28.57 (5)	28.57 (5)	28.57 (5)	28.57 (5)	28.57 (5)
Interpolation error	-	0 (0)	5.71 (1)	-10.71 (2)	0 (0)
Strain energy	-5.36 (1)	22.86 (4)	-10.71 (2)	-10.71 (2)	-10.71 (2)

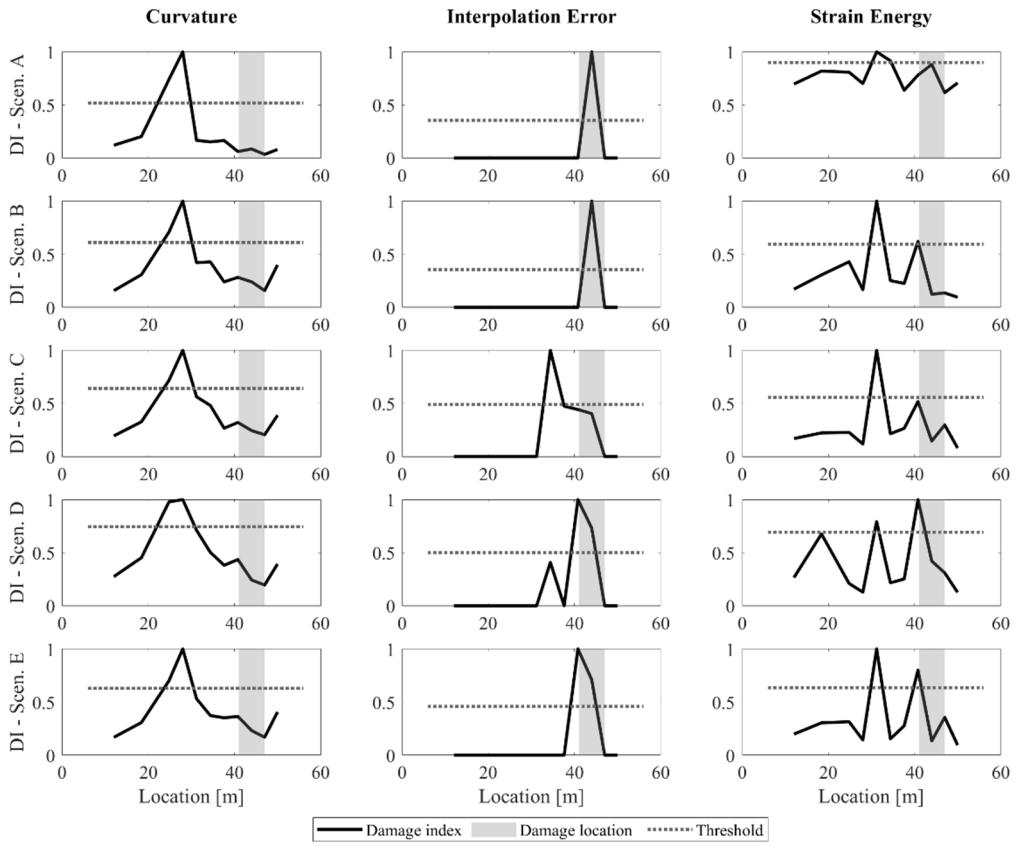

Figure A2: Damage features for different damage scenarios formulated in terms of ODSs (frequency range 0-20Hz)

Table A2. Relative error e_L [in %] using ODSs (frequency range 0-20 Hz)

Method	**Scenario**				
	A	**B**	**C**	**D**	**E**
Curvature	28.57 (5)	28.57 (5)	28.57 (5)	28.57 (5)	28.57 (5)
Interpolation error	0 (0)	0 (0)	17.14 (3)	5.71 (1)	5.71 (1)
Strain energy	22.86 (4)	22.86 (4)	22.86 (4)	5.71 (1)	22.86 (4)

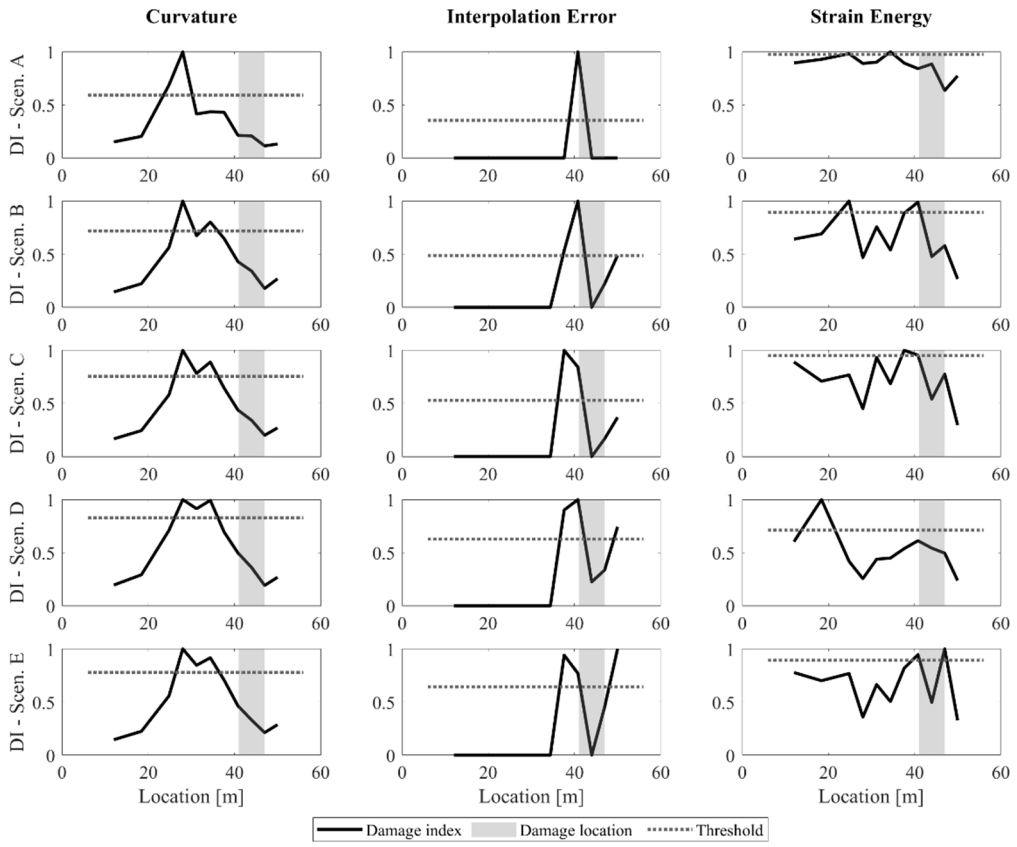

Figure A3: Damage features for different damage scenarios formulated in terms of ODSs (frequency range 0-40Hz)

Table A3. Relative error e_L [in %] using ODSs (frequency range 0-40 Hz)

Method	**Scenario**				
	A	**B**	**C**	**D**	**E**
Curvature	28.57 (5)	28.57 (5)	28.57 (5)	28.57 (5)	28.57 (5)
Interpolation error	5.71 (1)	5.71 (1)	11.43 (2)	5.71 (1)	-10.71 (2)
Strain energy	17.14 (3)	34.29 (6)	11.43 (2)	45.71 (8)	-5.36 (1)

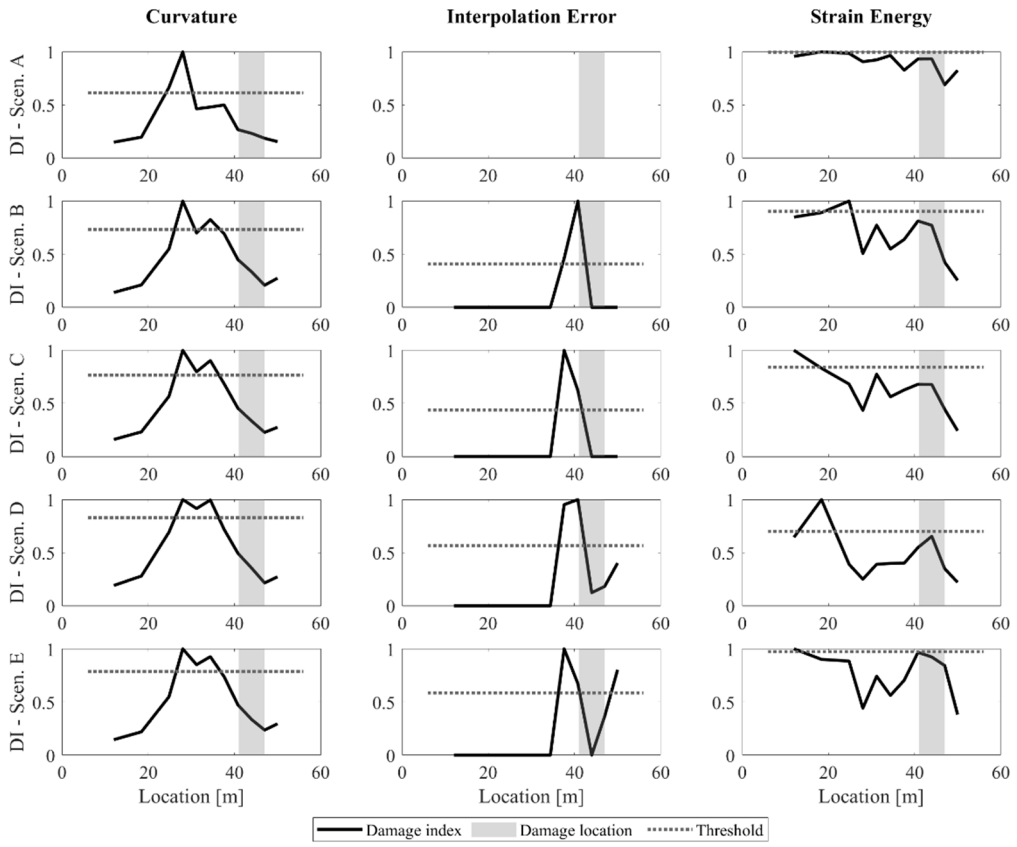

Figure A4: Damage features for different damage scenarios formulated in terms of ODSs (frequency range 0-50Hz)

Table A4. Relative error e_L [in %] using ODSs (frequency range 0-50 Hz)

Method	**Scenario**				
	A	**B**	**C**	**D**	**E**
Curvature	28.57 (5)	28.57 (5)	28.57 (5)	28.57 (5)	28.57 (5)
Interpolation error	-	5.71 (1)	11.43 (2)	5.71 (1)	11.43 (2)
Strain energy	45.71 (8)	34.29 (6)	57.14 (9)	45.71 (8)	57.14 (9)

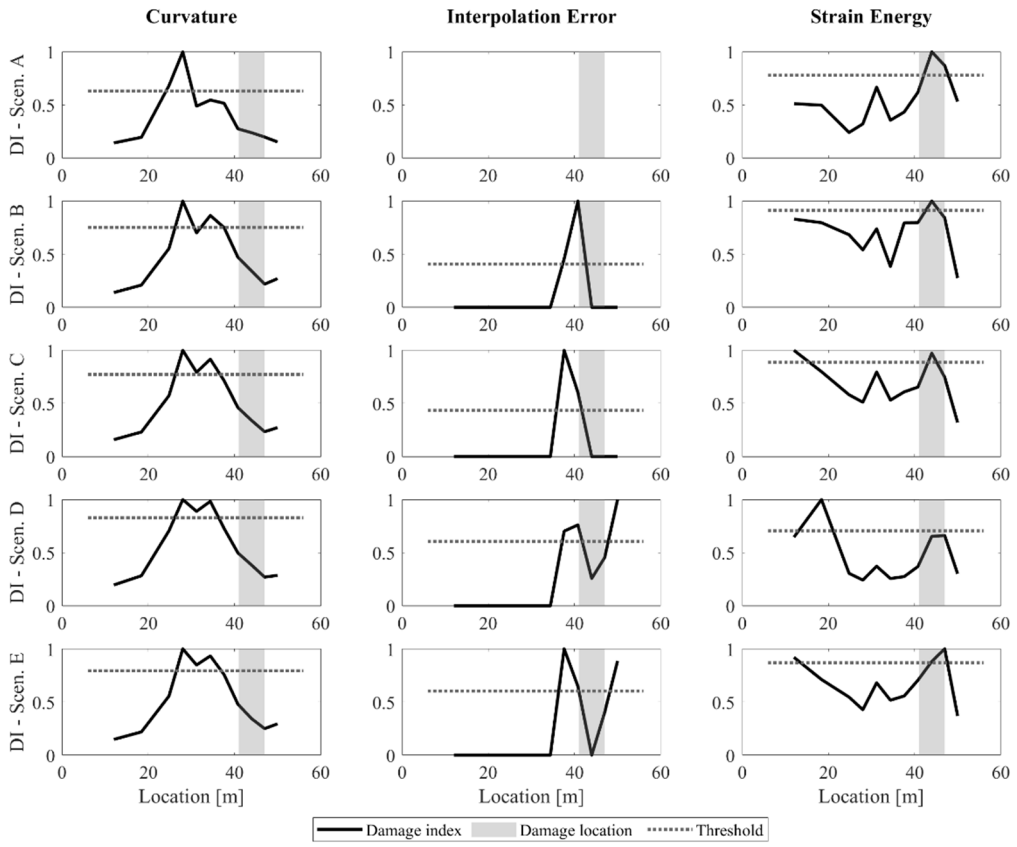

Figure A5: Damage features for different damage scenarios formulated in terms of ODSs (frequency range 0-100Hz)

Table A5. Relative error e_L [in %] using ODSs (frequency range 0-100 Hz)

Method	**Scenario**				
	A	**B**	**C**	**D**	**E**
Curvature	28.57 (5)	28.57 (5)	28.57 (5)	28.57 (5)	28.57 (5)
Interpolation error	-	5.71 (1)	11.43 (2)	-10.71 (2)	11.43 (2)
Strain energy	0 (0)	0 (0)	57.14 (9)	45.71 (8)	-5.36 (1)